Nanotechnology

LETTER

Conjugated π electron engineering of generalized stacking fault in graphene and *h*-BN

IOP Publishing Letters
Nanotechnology
Nanotechnology 29 (2018) 09LT01 (8pp) https://doi.org/10.1088/1361-6528/aaa663

Letter

Conjugated π electron engineering of generalized stacking fault in graphene and *h*-BN

Bin Ouyang[1,3], **Cheng Chen**[2] and **J Song**[2,3]

[1] National Center for Supercomputing Applications, University of Illinois at Urbana–Champaign, Urbana, IL 61801, United States of America
[2] Department of Mining and Materials Engineering, McGill University, Montreal, QC H3A 0C5, Canada

E-mail: bouyang@illinois.edu and jun.song2@mcgill.ca

Received 27 November 2017
Accepted for publication 9 January 2018
Published 29 January 2018

Abstract

Generalized-stacking-fault energy (GSFE) serves as an important metric that prescribes dislocation behaviors in materials. In this paper, utilizing first-principle calculations and chemical bonding analysis, we studied the behaviors of generalized stacking fault in graphene and *h*-BN. It has been shown that the π bond formation plays a critical role in the existence of metastable stacking fault (MSF) in graphene and *h*-BN lattice along certain slip directions. Chemical functionalization was then proposed as an effective means to engineer the π bond, and subsequently MSF along dislocation slips within graphene and *h*-BN. Taking hydrogenation as a representative functionalization method, we demonstrated that, with the preferential adsorption of hydrogen along the slip line, π electrons along the slip would be saturated by adsorbed hydrogen atoms, leading to the moderation or elimination of MSF. Our study elucidates the atomic mechanism of MSF formation in graphene-like materials, and more generally, provides important insights towards predictive tuning of mechanic properties in two-dimensional nanomaterials.

Supplementary material for this article is available online

Keywords: generalized stacking fault, graphene, conjugated π bond, dislocation

(Some figures may appear in colour only in the online journal)

1. Introduction

Atomic scale defects, including vacancies [1–5], dislocations [3, 6–8], stacking faults [9–11] and grain boundaries [3, 6, 8, 12, 13], in 2D materials can have a profound influence on the overall material behaviors, either as the origin of degradation that needs to be predicted and controlled, or as the source of new properties to be exploited [1, 14–17]. Therefore, it is highly desirable to understand the formation processes and function mechanisms of defects, and to be able to engineer the structure and distribution of them, in order to control or tune electronic properties [4, 18, 19], optical properties [13, 20, 21], and mechanical properties [7, 18, 22–26].

Recently, particular concern has been placed on dislocation behaviors in 2D materials, such as graphene [9, 13, 18] and hexagonal boron nitride (*h*-BN)[6, 17, 27]. For instance, the dislocations were shown to introduce dispersive impurity levels within materials and therefore modify the electronic band structure of materials [6, 8, 27–31]; Moreover, lattice distortion could induce formation of dangling bonds and trapping states, thus consequently altering the

[3] Authors to whom any correspondence should be addressed.

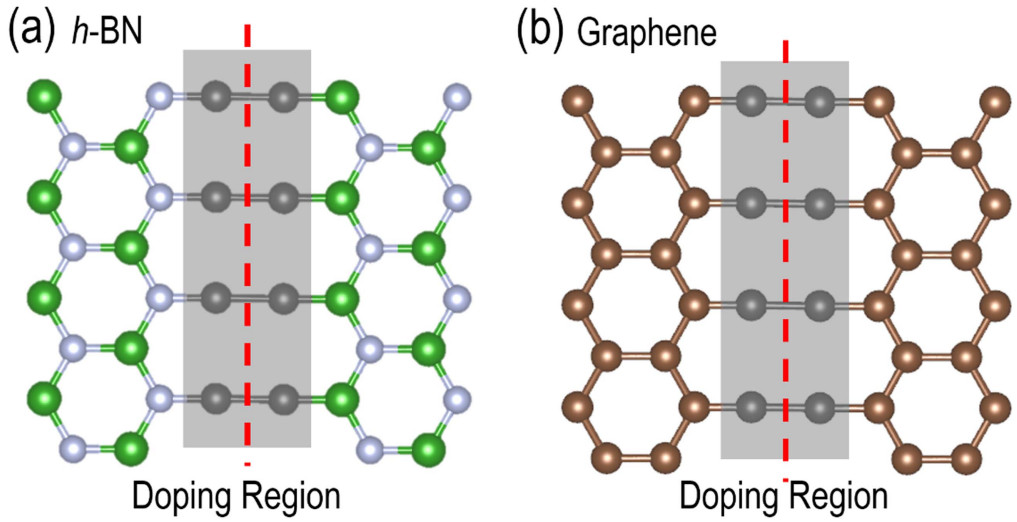

Figure 1. Illustration of atomic structure at slip displacement $\delta = 0.5b$ for (a) graphene; (b) *h*-BN.

magnetic and transport properties within these materials [3, 6, 20, 29, 32].

A critical metric in understanding dislocation behaviors in materials combining atomistic and a continuum scale is the Peierls−Nabarro model [10], in which the generalized-stacking-fault energy (GSFE) curve is required. The GSFE represents the energy cost associated with the shear displacement of dislocation slip. It plays a key role in prescribing the core structure and slip characteristics of dislocations. The GSFE curve can also serve as an essential input for the Peierls −Nabarro model [10] to enable continuum description of dislocations.

In the present study, GSFE profiles of graphene and *h*-BN were studied, considering the effect of doping (i.e., B and N doping of graphene, and C doping of *h*-BN). It was demonstrated that the formation of metastable stacking fault (MSF) in GSFE are strongly connected to the π conjugated bonds along the slip line, which can be further tuned via chemical functionalization such as hydrogenation. Our findings suggest that the dislocation characteristics and subsequent deformation behaviors in graphene like materials, may be regulated by chemically modification.

2. Methodology

Graphene and *h*-BN nanoribbons of width around 3 nm have been constructed for our DFT calculations. The lattice constants of graphene and *h*-BN are obtained to be 2.46 Å and 2.52 Å respectively, consistent with previous studies [1, 2, 4, 12, 13, 33] in the literature. The nanoribbons are separated from its periodic image along the armchair direction by a vacuum region of 2 nm, which has been confirmed to sufficiently eliminate image interactions. In all the simulation cells, two periodic units are used in periodic dimensions. Since we are particularly interested in the local atomic bonding at the center region of stacking fault, the length along the periodic direction would not affect the conclusions of our results.

For both graphene and *h*-BN, we focused on the glide slip, i.e., dislocation slip occurring across zigzag bonds, as shown in figure 1. Note that there are other common crystallographic directions, which were not considered here because the those slip directions cannot provide the local atomic environment for conjugated π bond forming (illustrated in figure S1, available online at stacks.iop.org/NANO/29/09LT01/mmedia in the supplementary information). To obtain the GSFE curve, the atoms on one side of the slip line were incrementally shifted with respect to the other side, and the associated energy cost per unit displacement was monitored. The procedure of displacement and subsequent relaxation are in accordance with previous studies [9, 10, 34]. When examining the effect of doping, common dopants, i.e., B and N in graphene and C in *h*-BN [9, 33], were considered. The introduction of dopants would only affect the chemical bonding of substituted atom with its nearest neighboring atoms. Therefore, the concentration variation, as well as coexistence of dopants, would certainly affect the amount of computed energies, but will not offer new types of local bonding configurations. Since we are focusing on the orbital overlapping of atoms due to formation of stacking fault, both concentration variation and coexistence of dopants will not affect the conclusions made. As a result, when it comes to doping conditions, we replaced all the sublattice atoms at the center region of the stacking fault (as shown in figure 1). Below, we denote N and B doping in graphene as C_N and C_B, respectively, while the substitution of N and B by C atoms in *h*-BN as N_C and B_C respectively, for ease of description.

Spin polarized DFT calculations were performed using the Vienna *ab initio* simulation package (VASP) [3] with projector augmented-wave (PAW) [1, 31, 35–37] pseudopotentials. The exchange correlation functions are approximated by generalized gradient approximation (GGA) of Perdew, Burke, and Ernzerhof (PBE). In each calculation, the energy cutoff is set as 500 eV while $1 \times 5 \times 1$ K mesh is applied. Both energy cutoff and k points have been benchmarked with larger values showing neglected energy difference (<0.01 eV).

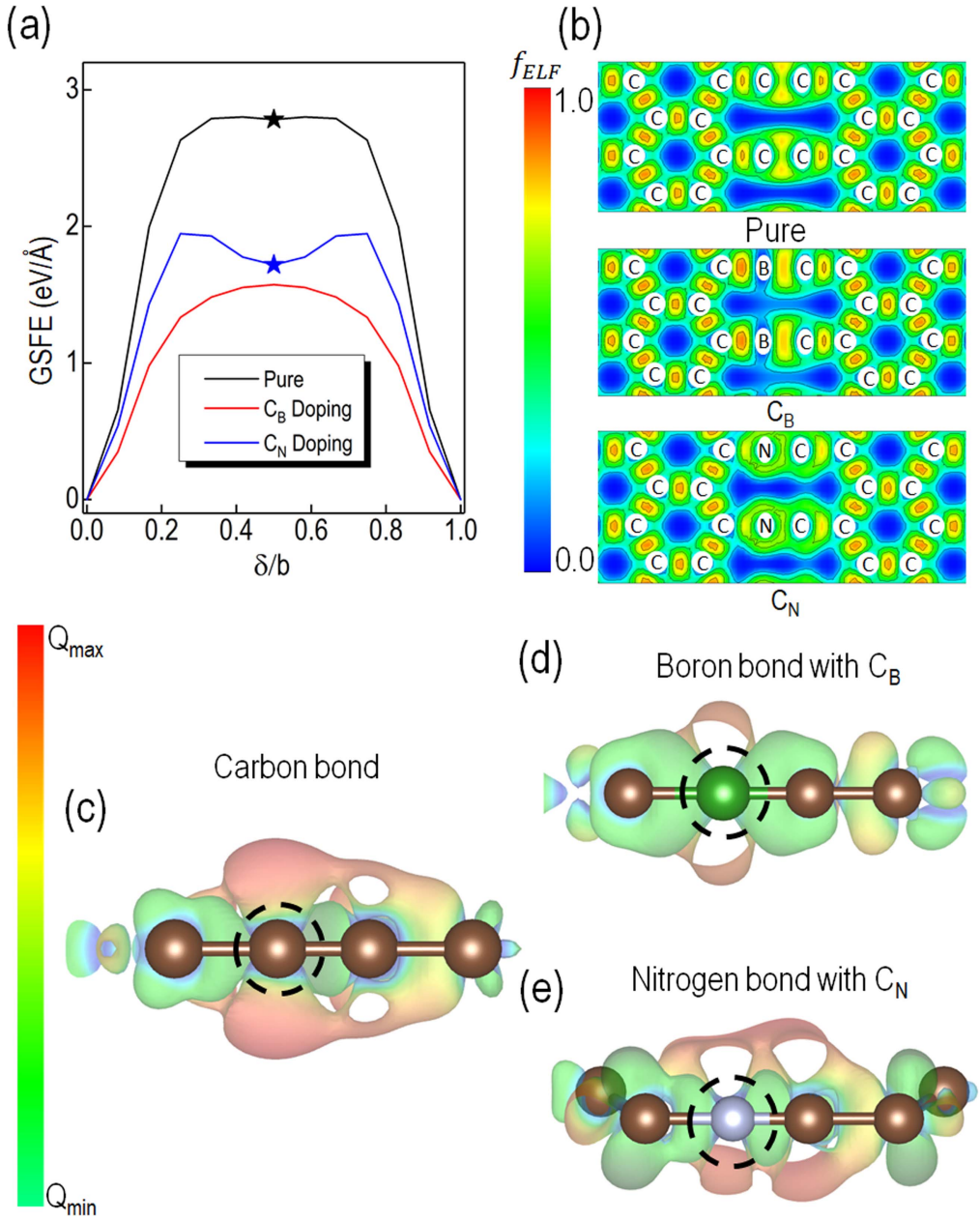

Figure 2. (a) The GSFE profiles along the slip direction for pristine, B-doped (C_B) and N-doped (C_N) graphene. The MSFs are indicated with the symbol star; (b) corresponding electron localized function plots at slip displacement $\delta = 0.5b$. (c)–(e) The deformation charge density plots illustrating the local bonding configurations across the slip line for pristine, B-doped (C_B) and N-doped (C_N) graphene, respectively, the isosurfaces are colored by calculated electrostatic potential and the key bonding atoms are indicated by dotted circles. The C, B and N atoms are respectively colored gray, green and light blue.

3. Results and discussions

3.1. GSFE profiles and bonding configurations in graphene

The computed GSFE profiles are demonstrated in figure 2(a). It can be seen from these profiles that there exists a metastable stacking fault (MSF), γ_{sf}, signified by the local minimum in the GSFE curve at slip displacement $\delta = 0.5b$ with b being the magnitude of the Burgers vector, for the pristine and N-doped graphene. On the other hand, for the case of B doping along the slip line, the MSF is absent in the GSFE curve.

To understand the formation of MSF and its relation to the local bonding configuration, we examined the electron localization function f_{ELF} which can be formulated as:

$$f_{ELF} = 1/(1 + \chi_\sigma^2(r)). \quad (1)$$

The χ_σ in equation one refers to the dimensionless localization index (details are provided in the supplementary information). As expected from equation (1), the value of f_{ELF} stays in the range [0, 1]. Generally, when an electron delocalizes at certain sites, f_{ELF} would have a value close to 0. On the other

hand, in the case of electrons being strongly localized, f_{ELF} would approach 1. As demonstrated in figure 2(b), it is obvious for pure graphene that the electrons around the C-C bond along the slip are localized, not only in the space between two C atoms, but also in the space around them. Similar phenomenon can be observed for N doping along the slip line (denoted as C_N in figure 2). However, in the case where C atoms along the slip line are substituted by B atoms, the electrons are only localized at the space between C and B atoms (see figure 2(b)).

To better visualize and understand the local bonding, the deformation charge density has been also computed, by cutting the isosurface from the center of C atoms in the line perpendicular to the slip direction. The resultant bonding configurations (at $\delta = 0.5b$) are demonstrated in figures 2(c)–(e) for the three systems considered. The electrostatic potential is calculated and used for surface coloring so that the density of electron at certain location can be directly viewed from the color scheme. From figure 2(c), the electron clouds from C atoms not only forms head-on overlapping, but also overlapping at the space around. The 'head to head' bonding can be attributed to the σ bond, while the overlapping aside from σ bonds delocalize slightly away from the atoms but the isosurface wrap two bonding atoms, which satisfy the feature of π bonds. When comes to C_N conditions, the existence of orbital overlapping with both σ and π features are also observed, which indicates similar bonding situation as the pure graphene case. However, when C atoms are substituted by B atoms, only head-on orbital overlapping can be observed between C and B atoms, while the π bond feature of electron cloud is absent.

The above observations suggest that those GSFE profiles illustrated in figure 2(a) can be understood in terms of local bonding configurations. When the graphene lattice is shifted by $\delta = 0.5b$ along the glide slip, conjugated π bonds would form in the pure and N-doped graphene systems. When comes to B-doped system, the π bond formation is absent. The reason underlying the above distinction in the bonding configuration can be obviously explained by the valence electrons of C, B, and N systems. For C and N atoms, there are 4 and 5 valence electrons in the outer shell so that the dangling electrons at stacking fault can be excited to form π bond, which will release energy and thus make the configuration metastable. On the other hand, B atom has only 3 valence electrons in the outer shell, which is insufficient for conjugated π bond formation.

3.2. GSFE profiles and bonding configurations in h-BN

Being an isomorph of graphene, *h*-BN possesses an identical lattice structure but different electronic structure. As shown in figure 3(a), the GSFE curves of pristine *h*-BN and N_C-doped *h*-BN along the glide slip exhibit no MSF. However, MSF is present (at $\delta = 0.5b$) in the GSFE curve of the B_C-doped *h*-BN.

Figure 3(b) shows the f_{ELF} contour for pristine and C-doped *h*-BN to illustrate the electron distribution around the slip line at $\delta = 0.5b$. Examining the triplet atomic line (i.e., N-B-N, N-C-N and N-B-C, see figures 3(c) and (d)) across the slip, we see that only under B_C doping, the electron distribution wrap up the three atoms at the triplet atomic line. The local bonding configurations across the slip line are further illustrated by the deformation charge density plots in figures 3(c) and (d). We note that σ and π bonds coexist at the triplet atom line N-C-N (see figure 3(c)) in the case of B_C doping, presumably induced by the introduction of an extra valence electron contributed by the substitution of a C atom. On the other hand, the formation of the π bond is not observed in the cases of pristine and C_N doped *h*-BN due to the lack of valance electrons in B atoms. Consequently, the conjugated π bond formation resulted in energy release and MSF only occurs for the B_C-doped *h*-BN.

3.3. Engineering GSFE through hydrogenation

The connection between the conjugated π bonding and MSF for graphene and *h*-BN provides intriguing hints towards engineering the GSFE and subsequently dislocation slip characteristics within graphene-like 2D materials. In the following we demonstrate that the GSFE can be further manipulated through adsorption of atoms for altering the π bond. In particular, we focus on hydrogenation, which is easy to realize and commonly used in graphene and *h*-BN systems [38–43], as a representative.

A schematic illustration of the hydrogenation process is given in figure 4(a). In this design, the tendency of hydrogen adsorption can be controlled by adjusting the hydrogen chemical potential (or equivalently the partial pressure of hydrogen gas). Meanwhile, the most favorable sites for hydrogen adsorption on MSF decorated graphene/*h*-BN can be inferred from local potential calculations. As demonstrated in figures 4(b)–(d), for three MSFs identified above (i.e. pristine graphene, graphene with C_N doping and *h*-BN with B_C doping), the local potentials are calculated with a line scan perpendicular to the slip direction. The relative energy taking vacuum (set as 0 eV in figures 4(b)–(d)) as a reference refers to the work function (indicated as W_F) of a specific spatial location, which describes the energy required to remove an electron from the system. In general, the lower value of W_F takes, the more active electrons in that site will be. As a result, the H adsorption activity of certain location in graphene/*h*-BN can be estimated from the local potential mapping[1]. Due to the periodicity and spacing of atom arrangement in the solids, the calculated local potential fluctuates along the direction perpendicular to the slip line. The upper enveloping line is chosen for demonstration in figures 4(b)–(d). As illustrated by figures 4(b)–(d), for all three types of configurations discussed, the most active sites are observed in the location of MSFs. More specifically, for pristine graphene, the calculated minimum work function $W_F^{\min}$ is 3.51 eV for the MSF within pristine graphene, while for the other locations of graphene W_F turns out to be around 4.6 eV. As for graphene with C_N doping, the W_F at MSF sites can be as

[1] Note: The smaller the energy gap between specific site and vaccum, the more active the site will be.

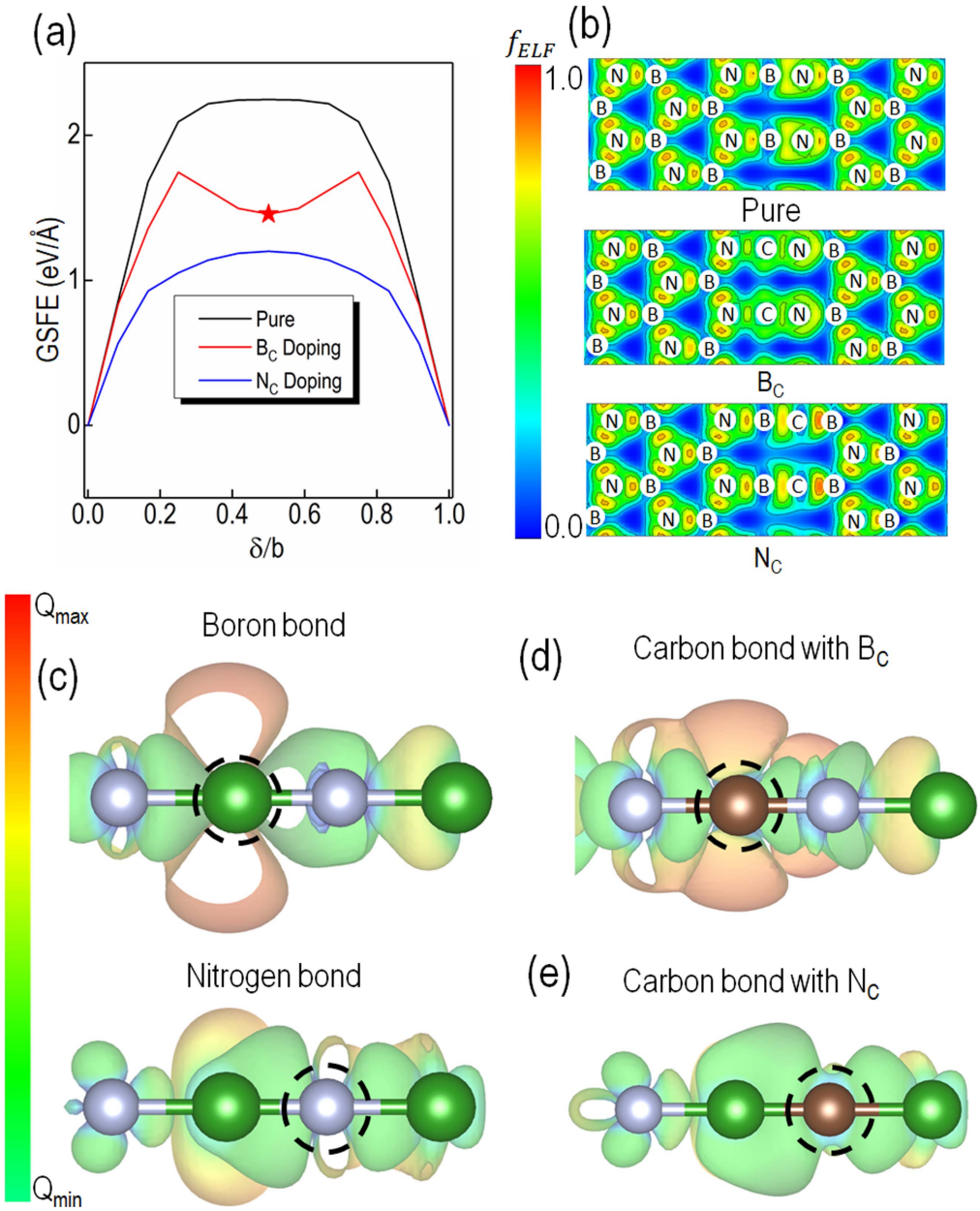

Figure 3. (a) The generalized stacking fault profile along the slip direction. The MSF is indicated with the symbol star; (b) electron localized function plot of three types of stacking fault configurations; (c)–(e) bonding analysis of the MSF in the slip direction of *h*-BN. The bonding atoms are indicated by dotted circle. The isosurfaces are colored by a calculated electrostatic potential. (c) The shape of boron bonds and nitrogen bonds in pristine *h*-BN; (d) the shape of carbon bond with the B_C substitution; (e) the shape of carbon bond with the N_C substitution.

low as 2.99 eV, while other sites far away from the MSF region have the value around 4.6 eV. When it comes to *h*-BN in B_C doping, the W_F at MSF sites turns out to be 4.4 eV, while in the other sites the value is around 6.22 eV. All those comparisons indicate that during hydrogenation procedure, H atoms tend to get absorbed near MSFs and interact with conjugated π bonds. Meanwhile, as reported by previous theoretical and experimental studies, the small reaction barrier for H diffusion [44–46] in graphene and *h*-BN will also make the aggregation of H kinetically favorable.

With the possibility of controllable H adsorption, the GSFE profiles with hydrogenation are compared with the situations without hydrogenation (dehydrogenation). By observing the GSFEs in figure 4(b), it can be found that for pristine graphene, the slightly decrease of GSFE (around 0.02 eV/Å) at $\delta = 0.5$b disappear after the adsorption of hydrogen atoms. As a result, MSF will disappear. Additionally, the calculated isosurface of deformation charge calculations embedded, clearly demonstrates the change of bonding configurations. It is obvious that with the adsorption of H atoms, the conjugated π bond disappears as a result. Similarly, for graphene with C_N, as shown in figure 4(c), MSF will gradually disappear accompanied by the hydrogenation process. When it comes to *h*-BN stacking fault with B_C doping as demonstrated in figure 4(d), the MSF will not disappear completely even with all C atoms decorated with

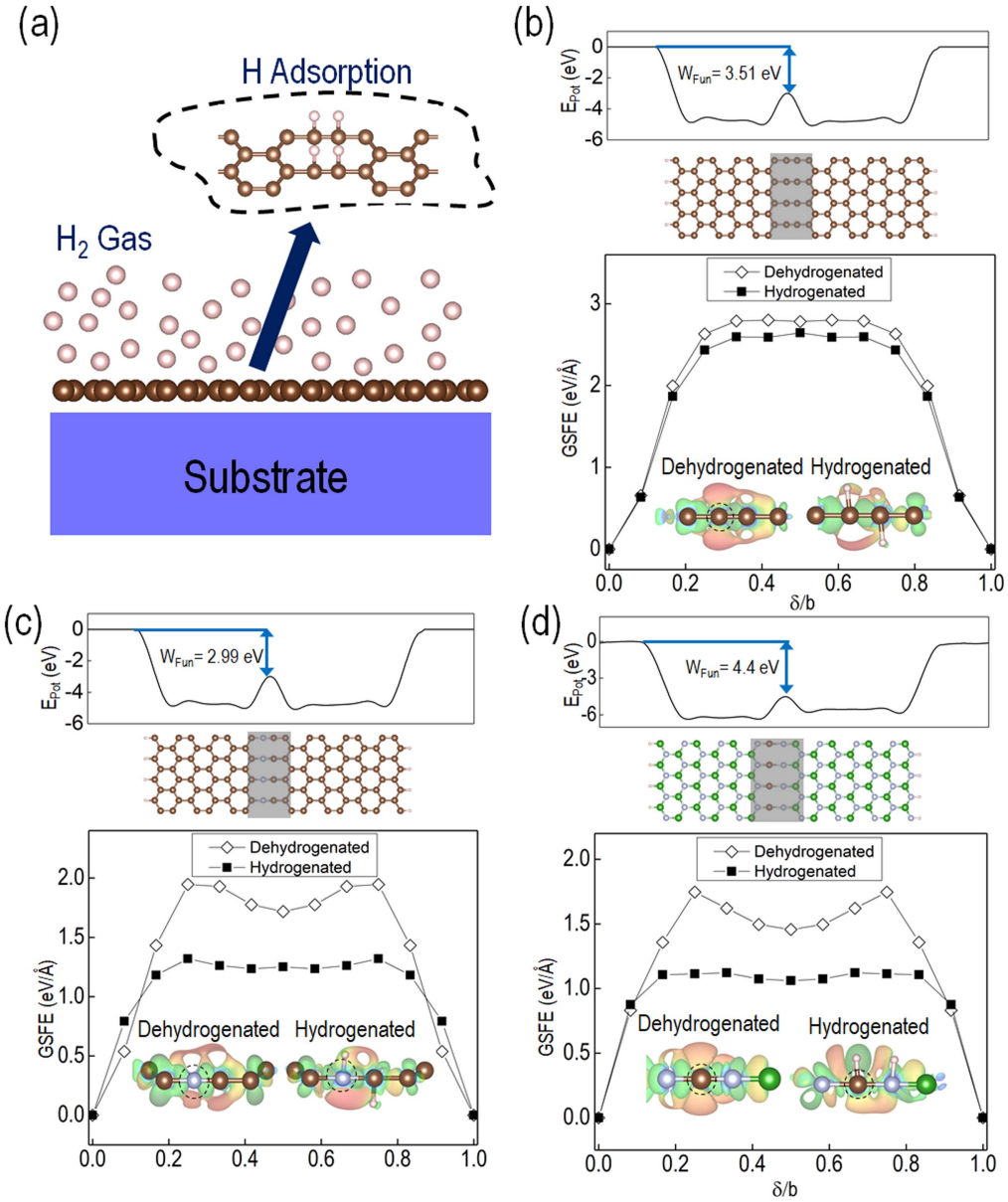

Figure 4. (a) Schematic illustration of the hydrogenation/dehydrogenation process. (b)–(d) The figures on top illustrates the local potential distribution of graphene or *h*-BN with MSF, with the correspondent atomic configurations given in the middle figures, while the resultant GSFE profiles under hydrogenation and dehydrogenation are shown in the bottom figures, with the systems being respectively: (b) graphene without doping; (c) graphene with C_N doping and (d) *h*-BN with B_C doping.

one hydrogen atom. However, the energy release due to forming of MSF decrease from 0.75 eV/Å to 0.06 eV/Å, that indicates a great weaken of conjugated π bonds due to hydrogenation. This phenomenon can also be confirmed with the corresponding deformation charge density plot.

The information from figure 4 elucidates the fact that with hydrogenation, the π electrons will be saturated by H atoms adsorption. As a result, the MSFs in graphene and *h*-BN would disappear or be significantly weakened. This confirm the possibility of controlling dislocation behavior of graphene-like materials with chemical functionalization. As demonstrated in our first principle theoretical study, the overall procedure is precisely controllable and reversible with the tuning of chemical potential of functionalization atoms. Therefore, our theoretical investigations will hopefully provide some new insights in tuning the mechanical properties and behaviors in graphene like 2D materials.

4. Conclusions

In summary, we studied GSFE curves along dislocation slips within graphene and *h*-BN, considering the effect of doping (i.e., B and N doping of graphene, and C doping of *h*-BN) employing first-principles calculations together with chemical bonding analysis. The existence of MSF in those materials was shown to be strongly connected to the formation of the conjugated π bond. Chemical functionalization was proposed as a possible means to engineer the local bonding configuration along the slip line, demonstrated with hydrogenation

as an example. In hydrogenation, hydrogen atoms were shown to preferentially adsorb along the faulted slip line where more active sites exist, therefore allowing targeted functionalization and tailoring of the local bonding configuration. As a consequence of hydrogenation, π bonds can be gradually saturated which can finally lead to the disappearance of MSF. Our findings clarify the atomistic origin underlying MSF in graphene-like materials, and provide important theoretical insights towards predictive tuning of dislocation behaviors, and consequently mechanic properties in graphene-like, and more generally two-dimensional nanomaterials.

Acknowledgments

We were grateful for the financial support from the McConnell Memorial Fellowship in Engineering, the McGill Engineering Doctorate Award, and the NSERC Discovery grant (# RGPIN 418469-2012). The authors also acknowledge the Supercomputer Consortium Laval UQAM McGill and Eastern Quebec for providing computing power.

ORCID iDs

Bin Ouyang https://orcid.org/0000-0002-8181-6815
Cheng Chen https://orcid.org/0000-0003-3062-9048

References

[1] Ouyang B, Meng F and Song J 2014 Energetics and kinetics of vacancies in monolayer graphene boron nitride heterostructures *2D Mater.* **1** 035007
[2] Song J, Ouyang B and Medhekar N V 2013 Energetics and kinetics of Li intercalation in irradiated graphene scaffolds *ACS Appl. Mater. Interfaces* **5** 12968–74
[3] Banhart F, Kotakoski J and Krasheninnikov A V 2011 Structural defects in graphene *ACS Nano* **5** 26–41
[4] Ouyang B and Song J 2013 Strain engineering of magnetic states of vacancy-decorated hexagonal boron nitride *Appl. Phys. Lett.* **103** 102401
[5] Ouyang B and Song J 2016 Tuning magnetic states of planar graphene/h-BN monolayer heterostructures via interface transition metal-vacancy complexes *J. Phys. Chem.* C **120** 23529–35
[6] Liu Y, Zou X and Yakobson B I 2012 Dislocations and grain boundaries in two-dimensional boron nitride *ACS Nano* **6** 7053–8
[7] Warner J H, Fan Y, Robertson A W, He K, Yoon E and Lee G D 2013 Rippling graphene at the nanoscale through dislocation addition *Nano Lett.* **13** 4937–44
[8] Yazyev O V and Louie S G 2010 Topological defects in graphene: Dislocations and grain boundaries *Phys. Rev.* B **81** 195420
[9] Meng F, Ouyang B and Song J 2015 First-principles study of dislocation slips in impurity-doped graphene *J. Phys. Chem.* C **119** 3418–27
[10] Ariza M P, Serrano R, Mendez J P and Ortiz M 2012 Stacking faults and partial dislocations in graphene *Philos. Mag.* **92** 2004–21
[11] Zhou S, Han J, Dai S, Sun J and Srolovitz D J 2015 van der Waals bilayer energetics: Generalized stacking-fault energy of graphene, boron nitride, and graphene/boron nitride bilayers *Phys. Rev.* B **92** 155438
[12] Zhang Z, Zou X, Crespi V and Yakobson B 2013 Intrinsic magnetism of grain boundaries in two-dimensional metal dichalcogenides *ACS Nano* **7** 10475–81
[13] Zhang Z, Yang Y, Xu F, Wang L and Yakobson B 2015 Unraveling the sinuous grain boundaries in graphene *Adv. Funct. Mater.* **25** 367–73
[14] Vancsó P, Márk G I, Lambin P, Mayer A, Kim Y, Hwang C and Biró L P 2013 Electronic transport through ordered and disordered graphene grain boundaries *Carbon* **64** 101–10
[15] Kraus J, Böcklein S, Reichelt R, Günther S, Santos B, Menteş T and Locatelli A 2013 Towards the perfect graphene membrane?—Improvement and limits during formation of high quality graphene grown on Cu-foils *Carbon* **64** 377–90
[16] Xia Y, Li Z and Kreuzer H J 2011 Adsorption, diffusion and desorption of hydrogen on graphene *Surf. Sci.* **605** L70–3
[17] Robertson A W *et al* 2015 Partial dislocations in graphene and their atomic level migration dynamics *Nano Lett.* **15** 5950–5
[18] Warner J H, Margine E R, Mukai M, Robertson A W, Giustino F and Kirkland A I 2012 Dislocation-driven deformations in graphene *Science* **337** 209–12
[19] Mesaros A, Sadri D and Zaanen J 2010 Parallel transport of electrons in graphene parallels gravity *Phys. Rev.* B **82** 073405
[20] Yazyev O V and Louie S G 2010 Electronic transport in polycrystalline graphene *Nat. Mater.* **9** 806–9
[21] Hao F, Fang D and Xu Z 2011 Mechanical and thermal transport properties of graphene with defects *Appl. Phys. Lett.* **99** 041901
[22] Polat E O, Balci O, Kakenov N, Uzlu H B, Kocabas C and Dahiya R 2015 Synthesis of large area graphene for high performance in flexible optoelectronic devices *Sci. Rep.* **5** 16744
[23] Fei Z *et al* 2013 Electronic and plasmonic phenomena at graphene grain boundaries *Nat. Nano* **8** 821–5
[24] Gong C, He K, Robertson A W, Yoon E, Lee G and Warner J 2015 Spatially dependent lattice deformations for dislocations at the edges of graphene *ACS Nano* **9** 656–62
[25] Grantab R, Shenoy V B and Ruoff R S 2010 Anomalous strength characteristics of tilt grain boundaries in graphene *Science* **330** 946–8
[26] Rasool H I, Ophus C, Zhang Z, Crommie M F, Yakobson B I and Zettl A 2014 Conserved atomic bonding sequences and strain organization of graphene grain boundaries *Nano Lett.* **14** 7057–63
[27] Nandwana D and Ertekin E 2015 Ripples, strain, and misfit dislocations: structure of graphene–boron nitride superlattice interfaces *Nano Lett.* **15** 1468–75
[28] Chen C, Wang Z, Kato T, Shibata N, Taniguchi T and Ikuhara Y 2015 Misfit accommodation mechanism at the heterointerface between diamond and cubic boron nitride *Nat. Commun.* **6** 6327
[29] Lee G, Yoon E, Hwang N, Wang C and Ho K 2013 Formation and development of dislocation in graphene *Appl. Phys. Lett.* **102** 021603
[30] Gutiérrez-Sosa A, Bangert U, Harvey A J, Fall C J, Jones R, Briddon P R and Heggie M I 2002 Band-gap-related energies of threading dislocations and quantum wells in group-III nitride films as derived from electron energy loss spectroscopy *Phys. Rev.* B **66** 035302

[31] Zou X, Liu Y and Yakobson B I 2013 Predicting dislocations and grain boundaries in two-dimensional metal-disulfides from the first principles *Nano Lett.* **13** 253–8
[32] Tang P, Zou X, Wang S, Wu J, Liu H and Duan W 2012 Electronic and magnetic properties of boron nitride nanoribbons with topological line defects *RSC Adv.* **2** 6192–9
[33] Ouyang B and Song J 2016 Covalent pathways in engineering h-BN supported graphene *Carbon* **98** 449–56
[34] Vítek V 1968 Intrinsic stacking faults in body-centred cubic crystals *Philos. Mag.* **18** 773–86
[35] Hohenberg P and Kohn W 1964 Inhomogeneous electron gas *Phys. Rev.* B **136** 864–71
[36] Kohn W and Sham L J 1965 Self-consistent equations including exchange and correlation effects *Phys. Rev.* A **140** 1133–8
[37] Blöchl P E 1994 Projector augmented-wave method *Phys. Rev.* B **50** 17953–79
[38] Silvi B and Savin A 1994 Classification of chemical bonds based on topological analysis of electron localization functions *Nature* **371** 683–6
[39] Savin A, Jepsen O, Flad J, Andersen O, Preuss H and Schnering H G V 1992 Electron localization in solid-state structures of the elements: the diamond structure *Angew. Chem. Int. Ed.* **31** 187–8
[40] Darvish Ganji M, Hosseini-khah S M and Amini-tabar Z 2015 Theoretical insight into hydrogen adsorption onto graphene: a first-principles B3LYP-D3 study *Phys. Chem. Chem. Phys.* **17** 2504–11
[41] Hu S *et al* 2014 Proton transport through one-atom-thick crystals *Nature* **516** 227–30
[42] Tozzini V and Pellegrini V 2013 Prospects for hydrogen storage in graphene *Phys. Chem. Chem. Phys.* **15** 80–9
[43] Johns J E and Hersam M C 2013 Atomic covalent functionalization of graphene *Acc. Chem. Res.* **46** 77–86
[44] Ivanovskaya V V, Zobelli A, Teillet-Billy D, Rougeau N, Sidis V and Briddon P R 2010 Hydrogen adsorption on graphene: a first principles study *Eur. Phys. J.* B **76** 481–6
[45] Kumar E M, Sinthika S and Thapa R 2015 First principles guide to tune h-BN nanostructures as superior light-element-based hydrogen storage materials: role of the bond exchange spillover mechanism *J. Mater. Chem.* A **3** 304–13
[46] Lueking A D, Psofogiannakis G and Froudakis G E 2013 Atomic hydrogen diffusion on doped and chemically modified graphene *J. Phys. Chem.* C **117** 6312–9